Radwan and Nagi
Bulletin of the National Research Centre (2022) 46:180
https://doi.org/10.1186/s42269-022-00870-5

Bulletin of the National Research Centre

RESEARCH

Open Access

Hydration behavior and formation of strätlingite compound (C_2ASH_8) in a bio-cement based on tri-calcium silicate and mono-calcium aluminate for dental applications: influence of curing medium

M. M. Radwan[1] and Shaymaa M. Nagi[2*]

Abstract

Background: The aim of this work was to study the influence of simulated body fluid (SBF) and Pseudomonas aeruginosa (in Mueller Hinton Broth, MHB media) on the hydration reactions, formation of strätlingite (C_2ASH_8) and morphology of a composite material based on nano-size tri-calcium silicate (C_3S) and tri-calcium aluminate (CA) phases. The two experimental phases were prepared in laboratory by firing the required molar ratios of chemically pure reactants by solid-state reactions at elevated temperatures. Investigation of setting time, micro-hardness, pH of immersion solution, X-ray diffraction analysis, infrared spectroscopy, scanning electron microscopy and cytotoxicity were also carried out.

Results: The results emphasized that the hydrated compounds of C_3S phase can partly solve the problem of conversion process through the formation of the more stable and highly mechanical stratlingite hydrate (C_2ASH_8) plates that results in an increase in hardness values for samples cured in distilled water (DW) at 37 °C. The SBF solution showed more strength loss than those cured in Pseudomonas aeruginosa microbe (MHB) medium bacterial solution. SEM and EDAX analyses emphasized the formation of hydroxyapatite at 37 °C.

Conclusions: The prepared cements are promising for dental application.

Keywords: Tri-calcium silicate, Mono-calcium aluminate, Calcium silicate, Hydrate, Strätlingite, Cytotoxicity

Background

Calcium silicate and calcium aluminate cement materials have been successfully improved for use in dentistry. The cements products have many beneficial properties: compressive strength, purity, suitable working and setting times, radiopacity, sealing and film thickness that meet the dental standard. Both cements have antimicrobial action due to their high pH curing media (Huang et al. 2019). They also have biomineralization property that came from the release Ca^{2+} and OH^- ions when contact with moist tissue. The released ions interact with tissue fluids phosphate ions, thus precipitating calcium phosphate compound (Camilleri 2014; Camilleri and Gandolfi 2010). Beside that both cements are known for their osteogenic property, which is considered an important property for pulpal and periapical tissues wound healing and bone health (Primus et al. 2022).

*Correspondence: smnagi@gmail.com

[2] Restorative and Dental Materials Department, Oral and Dental Research Institute, National Research Centre (NRC), 33 El Bohouthst. (Former El Tahrirst.), Dokki, Cairo 12622, Egypt
Full list of author information is available at the end of the article

Calcium aluminate cement (CA) has been considered for over two decades as one of the most common materials used in dental applications as it has suitable setting time and high early crushing strength at room temperature. The superior physico-mechanical properties of calcium aluminate cement during the first 24 h of hydration process makes it promising bio-dental material for different applications in dentistry (Parreiraet al. 2016). Hydration process of CA phase is highly dependent on the temperature of the reaction medium that is at 20 °C, CAH_{10} is the predominant hydration product, whereas at temperature higher than 20 °C, the main hydration phases are C_2AH_8 and AH_3 (Shanget al 2016; Ukrainczyket al 2007; Lee et al. 2001; Bushnell-Watson and Sharp 1986; Taylor 1990). Curing of Calcium aluminate cement in distilled water (DW) at temperature above 35 °C results in the conversion of the metastable CAH_{10} and C_2AH_8 hydrated compounds to the more stable cubic crystals of C_3AH_6 (hydrogarnet) and AH_3 (gibbsite) in a process called conversion. It was stated that the extent of conversion process increases by increasing the curing temperature and humidity of the curing medium as more metastable phases will dissolve resulting in the formation of the more stable compounds according to the following equations: (Taylor 1990; Luz and Pandolfelli 2012; Bushnell-Watson and Sharp 1986)

$$CA + 10H \rightarrow CAH_{10} \quad (1)$$

$$2CA + 11H \rightarrow C_2AH_8 + AH_3 \quad (2)$$

$$3CA + 12H \rightarrow C_3AH_6 + 2AH_3 \quad (3)$$

$$3CAH_{10} \rightarrow C_3AH_6 + 2AH_3 + 18H \quad (4)$$

$$3C_2AH_8 \rightarrow 2C_3AH_6 + AH_3 + 9H \quad (5)$$

The conversion process should be avoided as it increases the porosity and micro-cracks of the hardened pastes which will be responsible for the weak physical and mechanical properties (Luz and Pandolfelli 2012; Bushnell-Watson and Sharp 1986). It was found in a previous studies that the presence of free silica and calcium silicate hydrate (CSH) can partly inhibit the conversion process through formation of the more stable strätlingite compound (C_2ASH_8) that has good mechanical properties than hydrogarnet (C_3AH_6) in temperature range of 20–70 °C according to the following equations (Mostafa et al. 2012; Bentsen et al. 1990).

The ultra-pure tri-calcium silicate phase (C_3S) that is one of the two main calcium silicate phases present in mineral trioxide aggregate (MTA) was one of the cementitious materials used in dentistry (Lee et al. 1993; Lenji et al. 2017; Asgary et al. 2009). It exhibited adequate physico-mechanical properties in addition to good properties needed in dental applications such as good adhesion to tooth, bactericidal properties and bioactivity (Sarkar et al. 2005; Al-Haddad et al. 2017; Accorinte et al. 2008; Asgary and Kamrani 2008). Tri-calcium silicate (C_3S) phase is a hydraulic cement that can undergo setting and hardening processes in wet curing media such as distilled water (DW), saliva, blood, simulated body fluid (SBF), bacterial media and dentinal fluid through the formation of calcium silicate hydrate (CSH) gel once mixed with water according to the following chemical equation (Lee et al. 1993; Moreno-Vargasa et al. 2017; Camilleri 2007).

$$\underset{C_3S}{3CaO.SiO_2} + \sim 5.3H_2O \rightarrow \sim \underset{(CH)}{7CaOSiO_2.4H_2O} + \sim 1.3Ca(OH)_2 \quad (6)$$

Tri-calcium silicate phase (C_3S) has a relatively prolonged setting time which is not recommended in clinical and dental applications. This may be improved by mixing C_3S phase with calcium aluminate phase (CA) as it has fast setting and hardening processes (Lee et al. 1993). On the other hand, mixing of C_3S with CA phase may compensate the conversion process of the main aluminate hydrate compounds (CAH_{10} and C_2AH_8) at higher curing temperature by a reactions between CSH hydrate and amorphous free silica (SiO_2) present in C_3S phase powder with CAH_{10} and C_2AH_8 forming the more stable strätlingite compound (C_2ASH_8) (Taylor 1990; Bentsen et al. 1990).

The current research work aims at studying the influence of different curing media, namely, simulated body fluid (SBF) and Pseudomonas aeruginosa (in Mueller Hinton Broth, MHB media) in comparison with distilled water (DW) on the hydration reaction characteristics and morphology of a composite material based on tri-calcium silicate (C_3S) and tri-calcium aluminate (CA). Investigation of setting time, micro-hardness, pH of immersion solution, X-ray diffraction analysis, infrared spectroscopy, scanning electron microscopy and cytotoxicity of the formulated bio-cement were also carried out.

Methods

Materials preparation and characterization

Tri-calcium silicate (C_3S) phase (17–27 nano-meter) was synthesized by firing molded cubes of 3:1 CaO/SiO_2 molar ratio using ultra-pure limestone and quartz (99.6% SiO_2), in the presence of 0.5% boric acid at 1000 °C for 2-h (Taylor 1990). The product was ground, remolded using carbon tetrachloride and fired at 1450 °C for 2-h. The firing process was repeated until completion of the reaction. The end product was checked for the presence of free lime. The mono-calcium aluminate (CA) phase (73–113 nano-meter) was prepared in laboratory by dry mixing 1:1 molar ratio of $CaCO_3$ (≈99.8%) and Al_2O_3 (99.6% Alumina). The required 2-inch cubes were pressed from the homogenized molar mixture to be ready for firing at 1000 °C for 2 h, and then the cooled material was ground and remolded with the aid of carbon tetrachloride and fired at 1500 °C for 6 h. The final phase agreed with some studies that emphasize the levels of $C_{12}A_7$ and CA_2 decreased while CA phase increased with temperature and time (Taylor 1990; Emaraet al 2018; Rivas Mercuryet al 2005). The synthesized materials were ground for 15 h in an agate mill until the desired grain size. There were investigated by X-ray diffraction to characterize the synthesized phase (Fig. 1). The particle diameter in nano-meter was determined with the aid of transmission electron microscope (JEM-1230) at 100 kV to evaluate the particle size (Fig. 2).

In this investigation, a composite of bio-cement was formulated from the prepared tri-calcium silicate (C_3S) and mono-calcium aluminate (CA) phases according to the following weight percentages:

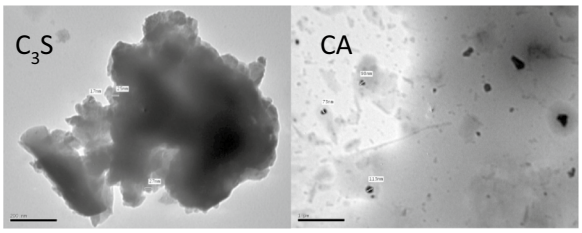

Fig. 2 Transmission electron photomicrographs (TEM) of tri-calcium silicate (nano-size C_3S phase: 17–27 nm) and calcium aluminate (nano-size CA Phase: 73–113 nm)

- 40 wt% C_3S phase.
- 40 wt% CA phase.
- 20 wt% chemically pure Bismuth Oxide (Bi_2O_3).

The homogenized dry composite material was finely ground for 3 h using Retsch GmbH PM100, Germany milling machine. One day hardened pastes were cured in incubator at 37 °C in the three curing media that are distilled water (DW), simulated body fluid (SBF) and Pseudomonas aeruginosa in Mueller Hinton Broth (MHB media). Preparation of a workable paste was done at a water/powder ratio of 0.23 ml/g. The paste sample was prepared using cylindrical mold of dimensions: diameter = 10 mm and height = 2 mm. It was poured in the mold in two equal layers, each layer was compacted and pressed in a homogenous specimen. After molding, the samples were cured in 100% humidity chamber at a constant temperature of 37 °C for 24 h. The samples were de-molded and cured in the different media at 37 °C until testing at 3, 7 and 14 days.

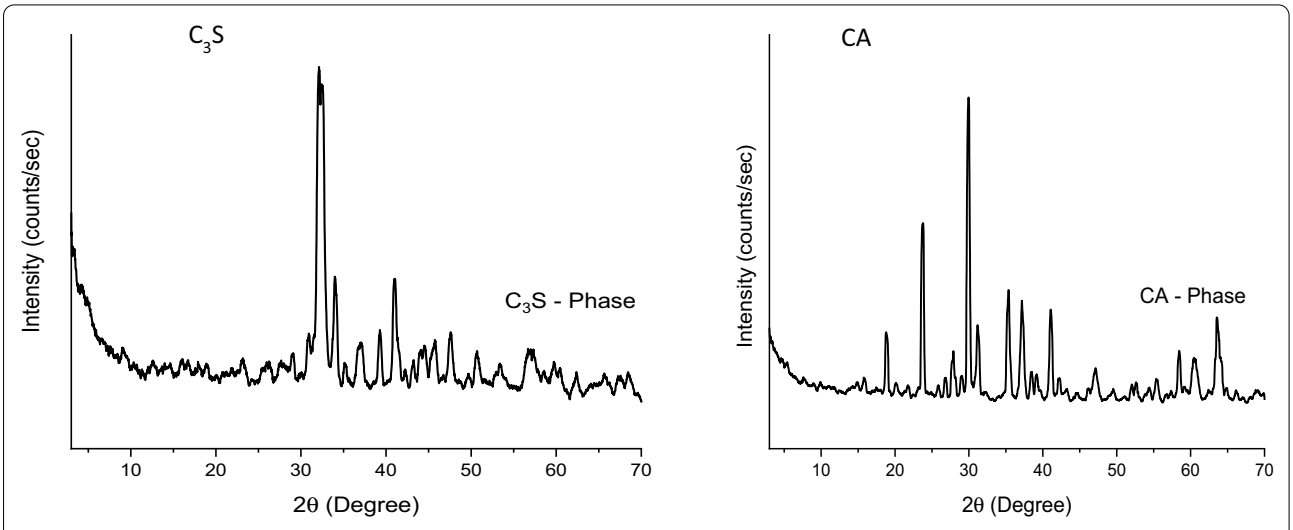

Fig. 1 X-ray diffraction patterns of tri-calcium silicate (C_3S) and calcium aluminate (CA) phases

Table 1 Ion concentration (mM) in the simulated body fluid (SBF) (Iftekhar et al. 2008)

Solution	Ion concentration (mM)							
	Na^+	K^+	Mg^{2+}	Ca^{2+}	Cl^-	HCO^{3-}	HPO_4^{2-}	SO_4^{2-}
SBF	141.9	5.01	1.5	2.5	147.8	4.2	1.0	0.5

- Preparation of SBF solution was done in laboratory according to Kokubo et al. (1990). The appropriate ratios of chemically pure NaCl, $NaHCO_3$, KCl, $K_2HPO_4.3H_2O$, $MgCl_2.6H_2O$, $CaCl_2$ and Na_2SO_4 were dissolved in deionized water at pH = 7.4 with the aid of Tris-(hydroxyl methyl)-amino methane $[(CH_2OH)_3CNH_3]$ and hydrochloric acid buffer solution as shown in Table 1.
- Incubation of the material was carried out in Mueller Hinton Broth media (Eliopoulus et al. 1989); 25 ml of the broth in 100 ml conical flasks was first sterilized and inoculated with 200 µl of Pseudomonas aeruginosa at 3.5 × 100 CFU/ml.
- The chemical composition of the media (Gram/Liter) is given as follows (Kokubo et al. 1990):
  - Beef infusion solids 2.0
  - Starch 1.5
  - Casein hydrolysate 17.0
  - pH after sterilization 7.4 ± 0.1
  - Temp. 25 °C

Setting time

The final setting time of the formulated bio-composite was carried out using Vicat apparatus using the past prepared with distilled water for 30 s at a water/powder ratio of 0.23 ml/g. The paste was poured into a disk mold of 10 mm diameter and 2 mm in thickness. After 120 s from the start mixing time, a Gilmore needle (with a flat end diameter of 2 mm and weighting 100 g load) was gently lowered to the surface of the tested sample. This procedure was repeated at 30-s intervals until the indenter failed to make a complete circular mark on the tested material. The recorded average setting time of set of five disk samples prepared from the synthesized composite bio-material was taken.

X-ray diffraction

The X-ray diffraction analysis was carried out on some selected hydrated samples with the aid of Philips X-ray diffractometer PW 1730 with Ni-filtered Cu-Kα X-ray radiation ($\lambda = 1.5406$ Å) powered at 40 kV and 30 mA. Diffraction data were recorded in the 2θ range from 5° to 70°, counting for 10 s in steps of $\Delta(2\theta) = 0.01°$.

ATR/FTIR spectroscopy

IR spectra were recorded on some selected samples with the aid of JASCO model FTIR 6100 spectrometer made in Japan in the range 4000–400 cm^{-1} with resolution 4 cm^{-1}.

SEM–EDS analysis

Investigation of the morphology of some selected cured samples was done by scanning electron microscopy (SEM) together with energy-dispersive X-ray spectra (EDX) using an instrument (type Inspect S, T810, D8571, FEI Co., Japan) with an accelerating voltage of 30 kV and a magnification from 10× to 300,000×.

pH of the immersion solution

Disk specimens of cement paste were prepared by mixing with distilled water for 30 s at a water/powder ratio of 0.25 ml/g. The workable mix was then placed in a mold that measured 10 mm diameter and 2 mm in thickness. Then, the prepared disks were directly placed in 20 ml of each curing medium mentioned above (Eliopoulus et al. 1989; Nurit et al. 1993) (and kept at 37 °C in a 100% humidity water bath for 3-, 7- and 14-day curing periods. The pH values of the immersion solution were determined using a solid-state pH sensor connected to a pH meter (Medika Scientific Jenway bench top pH meter, England).

Determination of calcium and phosphorus ions

The concentration of calcium and phosphorus ions released in the curing media were measured by Agilent 5100 Inductively Coupled Plasma–Optical Emission Spectrometer (ICP-OES) with Synchronous Vertical Dual View (SVDV). For each series of measurements intensity calibration curve was constructed composed of a blank and three or more standards from Merck Company (Germany). Accuracy and precision of the measurements were confirmed using external reference standards from Merck, and standard reference material for trance elements in water and quality control sample from National

Institute of Standards and Technology (NIST) were used to confirm the instrument reading (Wang et al. 2008).

Micro-hardness

Micro-hardness testing was performed at two different time intervals (24 h and 28 days). Ten specimens of 15 mm diameter and 2 mm thick were prepared using distilled water (DW) and allowed to cure for 24 h at 37 ± 1 °C in an incubator. The specimens were then removed from the molds and subjected for micro-hardness test (24 h) using Vickers micro-hardness tester (Nexus 4503, Innova Test, Netherlands, Europe). Three randomized indentations were made with a 100-g load, with a dwell time of 10 s. For randomization, specimens were arbitrarily rotated before indentations. Then, the tested specimens were randomly divided into two groups according to the immersion media; either immersed in 20 ml of each of DW, SBF and bacterial solution for 28 days. After immersion in the three curing media for 3, 7 and 28 days, the specimens were dried in a desiccator. The surface of each disk was ground using progressively finer grits of silicon carbide paper, from 180 to 1200 grit, and finally polished using 3-micron polycrystalline diamond paste. Then measurement of micro-hardness was performed again as mentioned before (APHA et al. 2017).

Cytotoxicity test

Cell culture

- Preparation of sample.

Black plastic sample was soaked in alone with media for 48 h in refrigerator, and then the media was added to the cell.

Cytotoxic effect on human normal fibroblast cell line (BJ1)

Cell viability was assessed by the mitochondrial dependent reduction of yellow MTT (3-(4,5-dimethylthiazol-2-yl)-2,5-diphenyl tetrazolium bromide) to purple formazan (Mosmann, 198).

- Procedure: All the following procedures were done in a sterile area using a Laminar flow cabinet biosafety class II level (Baker, SG403INT, Sanford, ME, USA). Cells were suspended in DMEM-F12 medium with1% antibiotic–antimycotic mixture (10,000U/ml Potassium Penicillin, 10,000 µg/ml Streptomycin Sulfate and 25 µg/ml Amphotericin B) and 1% L-glutamine at 37 °C under 5% CO_2.

Cells were batch cultured for 5 days and then seeded at concentration of 10 × 103 cells/well in fresh complete growth medium in 96-well microtiter plastic plates at 37 °C for 24 h under 5% CO_2 using a water jacketed carbon dioxide incubator (Sheldon, TC2323, Cornelius, OR, USA). Media was aspirated, fresh medium (without serum) was added, and cells were incubated either alone (negative control) or with different concentrations of sample to give a final concentration of (ug/ml). After 48 h of incubation, medium was aspirated, and 40 ul MTT salt (2.5 µg/ml) was added to each well and incubated for further 4 h at 37 °C under 5% CO_2. To stop the reaction and dissolving the formed crystals, 200 µL of 10% sodium dodecyl sulfate (SDS) in deionized water was added to each well and incubated overnight at 37 °C. A positive control which composed of 100 µg/ml was used as a known cytotoxic natural agent who gives 100% lethality under the same conditions.

The absorbance was then measured using a microplate multi-well reader (Bio-Rad Laboratories Inc., model 3350, Hercules, California, USA) at 595 nm and a reference wavelength of 620 nm. A statistical significance was tested between samples and negative control (cells with vehicle) using independent t test by SPSS 11 program. DMSO is the vehicle used for dissolution of plant extracts and its final concentration on the cells was less than 0.2%. The percentage of change in viability was calculated according to the formula: ((Reading of extract/Reading of negative control) − 1) × 100.

A probit analysis was carried out for IC50 and IC90 determination using SPSS 11 program (APHA et al. 2017).

Results

Setting time and microhardness

Evaluation of the final setting time was carried out on the material pastes of normal consistency prepared

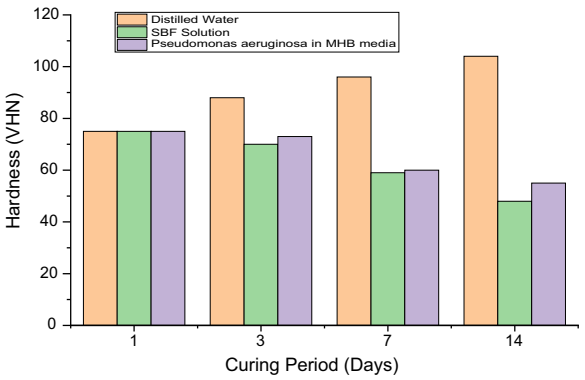

Fig. 3 Micro-hardness data of the hardened pastes cured in distilled water (DW), simulated body fluid (SBF) and Pseudomonas aeruginosa in Mueller Hinton Broth (MHB media)

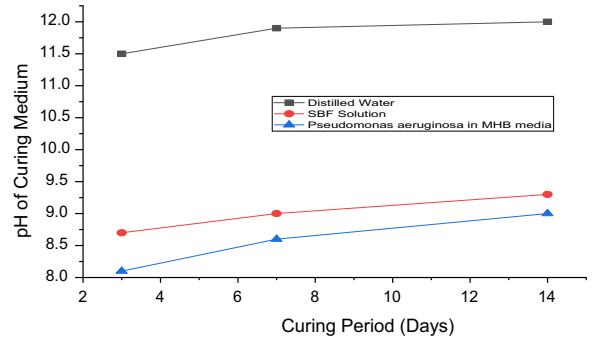

Fig. 4 pH values of distilled water (DW), simulated body fluid (SBF) and Pseudomonas aeruginosa in Mueller Hinton Broth (MHB media)

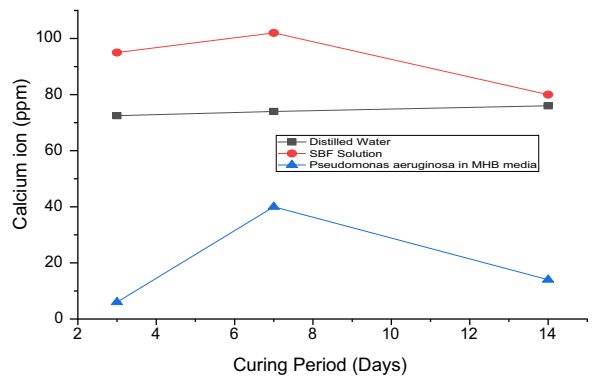

Fig. 5 Calcium ion concentration of distilled water (DW), simulated body fluid (SBF) and bacterial solution (MHB media) at different immersing periods

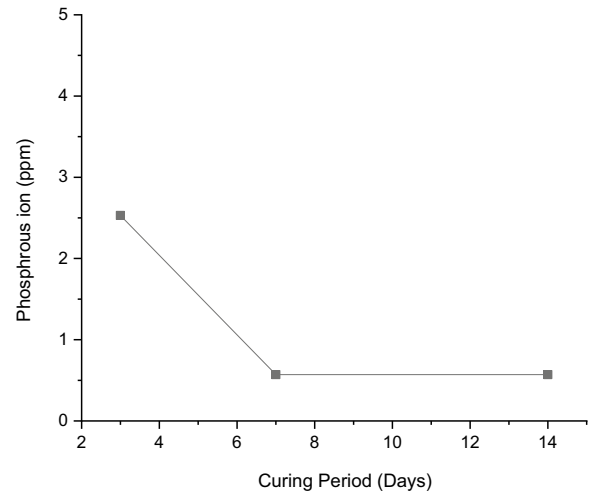

Fig. 6 Phosphorus ion concentration of Pseudomonas aeruginosa in Mueller Hinton Broth (MHB media) at different immersing periods

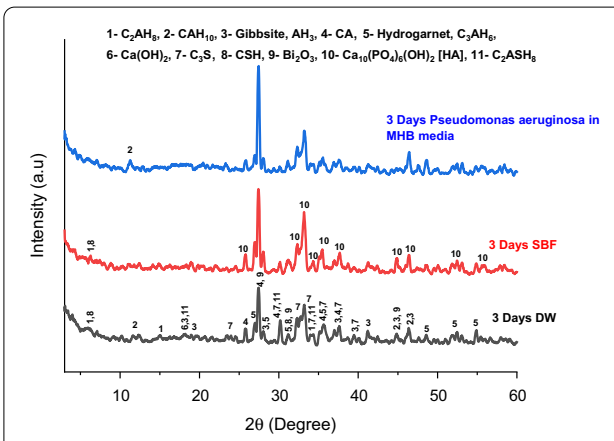

Fig. 7 X-ray diffraction patterns of 3-day sample cured in distilled water (DW) simulated body fluid (SBF) and Pseudomonas aeruginosa in Mueller Hinton Broth (MHB media)

with distilled water at a liquid/solid ratio of 0.23 ml/g as given in "Setting time" section. The recorded average setting time was 20 min at 37 °C (average of five readings). Figure 3 shows the hardness data of samples cured in the different hydration media at all curing ages. Figure 3 indicates that the hardness values of samples cured in distilled water (DW) increase with the hydration period from one day and up to 14 days, while for samples cured in SBF solution and the Pseudomonas aeruginosa microbe in MHB media there was a decrease in the hardness values at all curing ages. However, the samples immersed in the microbe medium showed slightly higher hardness values than those cured in SBF solution at all hydration periods.

pH of the curing media

The pH values of the curing media as a function of immersing ages are illustrated in Fig. 4. The pH data reveal that there is a little increase in the pH values of the three immersion liquids with the hydration period. As can be seen from Fig. 4, the samples cured in distilled water DW showed the highest pH values, while the lowest pH values were recorded for the samples cured in SBF solution.

Calcium and phosphorus ions

Figure 5 illustrates the concentrations of calcium ions present in the three curing media at all curing ages. Figure 5 shows that the values of Ca^{2+} ions concentrations were the highest for samples immersed in SBF solution followed by those stored in distilled water and those cured in the microbe media showed the lowest values. The calcium ion concentrations for the samples cured in both SBF solution and MHB media increased from 3 to

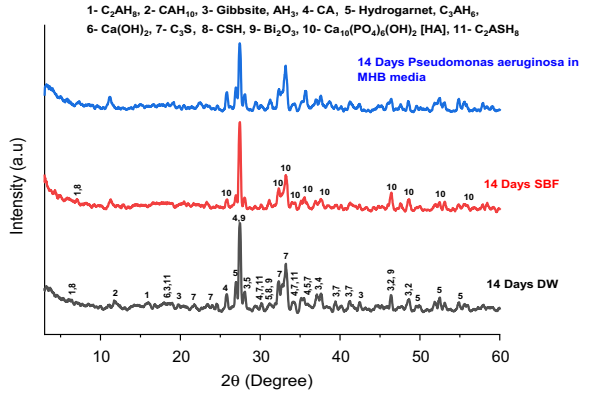

Fig. 8 X-ray diffraction patterns of 14-day sample cured in distilled water (DW) simulated body fluid (SBF) and Pseudomonas aeruginosa in Mueller Hinton Broth (MHB media)

7 days and then decreased at 14-day sample, while, for the sample cured in distilled water, these values showed very little or almost no change. The phosphorus ion concentrations present in the SBF solution are shown in Fig. 6. The data indicate a phosphorus ions decrease from 3- to 7-day samples followed with no change for the 14-day sample.

X-ray diffraction

Figures 7 and 8 represent the X-ray diffraction patterns of 3- and 14-day samples cured in distilled water (DW) in comparison with those cured in both SBF solution and Pseudomonas aeruginosa microbe medium. The characteristic peaks of the remaining anhydrous C_3S and CA particles could be detected in the XRD patterns shown in Figs. 7 and 8. Due to the complex hydration system of the formulated bio-composite, the overlapping of the some characteristics XRD peaks could be detected in all patterns. Investigation of Figs. 7 and 8 showed a decrease in the peaks heights of the anhydrous C_3S and CA phases for samples cured in the microbe MHB medium more than those cured in SBF solution comparing to the sample immersed in distilled water (DW). The XRD peaks of the main hydration products of calcium aluminate phase (CAH_{10} and C_2AH_8) were found in the patterns separate or overlapping with other peaks and they showed a slight peak height increase for the sample stored in microbe solution than for those cured in SBF solution for both 3- and 14-day samples. The X-ray diffraction peaks of gibbsite (AH_3) and hydrogarnet (CAH_6) are clearly detected, due to the conversion process of the main hydrated phase, CAH_{10} and C_2AH_8 in addition to those of strätlingite compound (C_2ASH_8) overlapped with other XRD peaks that is formed due to the expected reaction of the main hydrated compounds with the free silica present in C_3S phase and the calcium silicate hydrate (C–S–H) at 37 °C. They showed a lower peaks heights for the samples cured in the SBF solution. The X-ray diffraction peaks of calcium silicate hydrate (CSH) that is the hydrated phase of C_3S could be seen in all patterns but overlapping with other XRD peaks. The free lime [$Ca(OH)_2$] liberated during the hydration reactions of C_3S phase showed its XRD peak more clear for samples cured under distilled water (DW) with a minimum height for the sample cured in the MHB media. The XRD peaks characteristic for hydroxyapatite (HA) that may be formed on the surface of the hardened material immersed in SBF solution could be detected in the XRD pattern of samples cured in the SBF medium but overlapped with those XRD peaks characteristic for the phase in the same d-spacing making an increase in their heights as shown in Figs. 7 and 8.

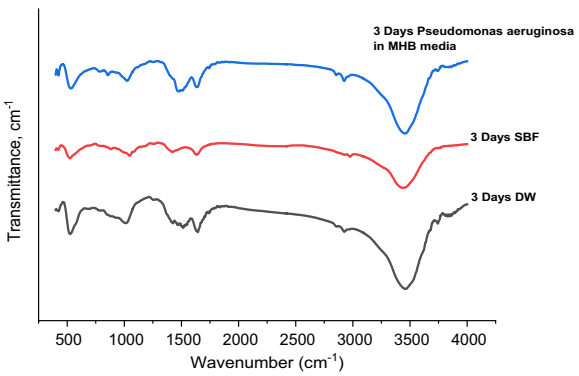

Fig. 9 FTIR spectral bands of 3-day sample cured in distilled water (DW) simulated body fluid (SBF) and Pseudomonas aeruginosa in Mueller Hinton Broth (MHB media)

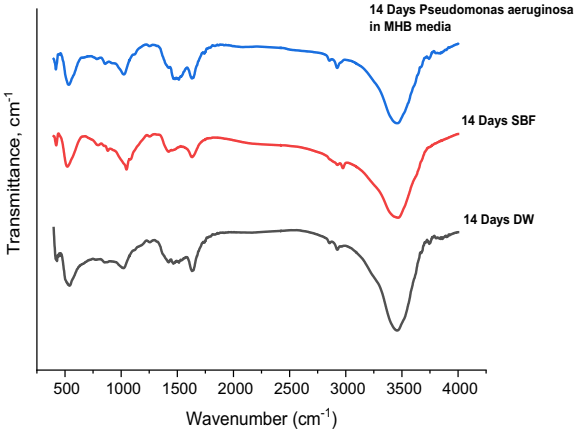

Fig. 10 FTIR spectral bands of 14-day sample cured in distilled water (DW) simulated body fluid (SBF) and Pseudomonas aeruginosa in Mueller Hinton Broth (MHB media)

Table 2 Results of FTIR analysis

Wave number (cm^1)	Crystal phase
850	$\upsilon_2\ CO_3^{2-}$ out of plane bending
1400–1500	$\upsilon_3\ CO_3^{2-}$ stretching vibrations
600–500	The vibration of $C_3AH_6$and may overlap with that of the Al–O_6
550–520 850–800	The Al–O vibrations
1100–1000	The absorption band of α-$Al(OH)_3$
970–990 1027	The O–H bending vibration attributed to gibbsite (AH_3)
3475, 3530 and 3630	The O–H stretching vibration attributed to gibbsite (AH_3)
524, 3465 and 3670	The bands appearing of the water hydrated CAC paste (CAH_{10}, C_2AH_8 and C_3AH_6)
1650–1600	The H–O–H bending vibration band of CAH_{10}
1100–1050	The symmetric stretching vibration of $\upsilon_3\ PO_4^{3-}$
650–560	The PO_4^{3-} bending vibration
445–815–950	CSH phase
491–667	Si–O–Si the main band corresponding to Si–O bond
490	$\upsilon_2\ OH^-$ stretching in $Ca(OH)_2$ or HAP
3648	Very broad OH^- absorption bands
2500–3700	OH^- band

FTIR spectroscopy

Figures 9 and 10 illustrate the FTIR spectral bands of the 3- and 14-day samples cured in SBF solution and the microbe in (MHB) media in comparison with those hydrated in distilled water (DW). Due to the complex hydration process of the synthesized bio-composite material which results in a many hydration compounds and byproducts that may cause overlapping of their IR bands, so, it was better to collect the results of FTIR analysis in Table 2. Investigation of the IR results illustrated in Table 2 and Figs. 9 and 10 showed the presence of the IR bands corresponding to the calcium silicate hydrate (CSH) at ≈ 445–815–950 cm^{-1} overlapping with those at ≈ 491–667 cm^{-1} for Si–O–Si bond which showed a maximum intensities for the sample cured in distilled water (DW) followed by those immersed in the microbe medium (MHB) and their minimum for the SBF solution. The main hydrated phases of calcium aluminate phase (CA) that are CAH_{10}, C_2AH_8 and C_3AH_6 showed their characteristic IR bands of their water molecules of hydration at ≈ 524–3465–3670 cm^{-1}. The bands corresponding to the vibration of C_3AH_6, Al–O_6 and Al–O are overlapping in the same transmittance wave length region of ≈ 500–600 cm^{-1} and at ≈ 800–850 cm^{-1} for Al–O vibration. The H–O–H bending vibration band of CAH_{10} was found at ≈ 1600–1650 cm^{-1}. The O–H bending vibration for the gibbsite (AH_3) can be seen at ≈ 970–1027 cm^{-1} and those attributed to the O–H stretching vibration also for the gibbsite is located at ≈ 3475–3630 cm^{-1}. The IR band at ≈ 1000–1100 cm^{-1} is attributed to α-$Al(OH)_3$. The IR bands characteristic for symmetric stretching vibration $\acute{\upsilon}_3PO_4^{3-}$ corresponding to the hydroxyapatite (HA) are overlapped in the region of 1050–1100 cm^{-1} and those corresponding to the bending vibration of PO_4^{3-} at the range of 560–650 cm^{-1}. The IR spectral data of the 14-day samples showed in Fig. 10 showed an increase in the bands' intensities that may be due to the formation of hydroxyapatite (HA) on the surface of the hardened paste sample. The characteristic IR bands of anti-symmetric stretching $\acute{\upsilon}_2$and $\acute{\upsilon}_3\ CO_3^{2-}$ ~850, 1400–1500 cm^{-1} were found all samples immersed in the bacterial solution, but they showed a very small shoulders for the one and 14-day samples of distilled water. The IR bands at ≈3648 and the broad band at ≈2500–3700 are mainly attributed to OH^- and hydration water (H_2O) molecules.

SEM–EDS analysis

Figure 11 illustrates the morphology features of the 14-day samples cured in distilled water (DW), simulated body fluid solution (SBF) and Pseudomonas aeruginosa microbe (MHB) medium. As can be seen from the SEM micrographs shown in Fig. 11, there is a clear difference in the microstructures of the three tested samples. The paste sample cured in SBF solution (Fig. 11, plate b) showed a more porous and weak microstructure than the other two samples. The sample

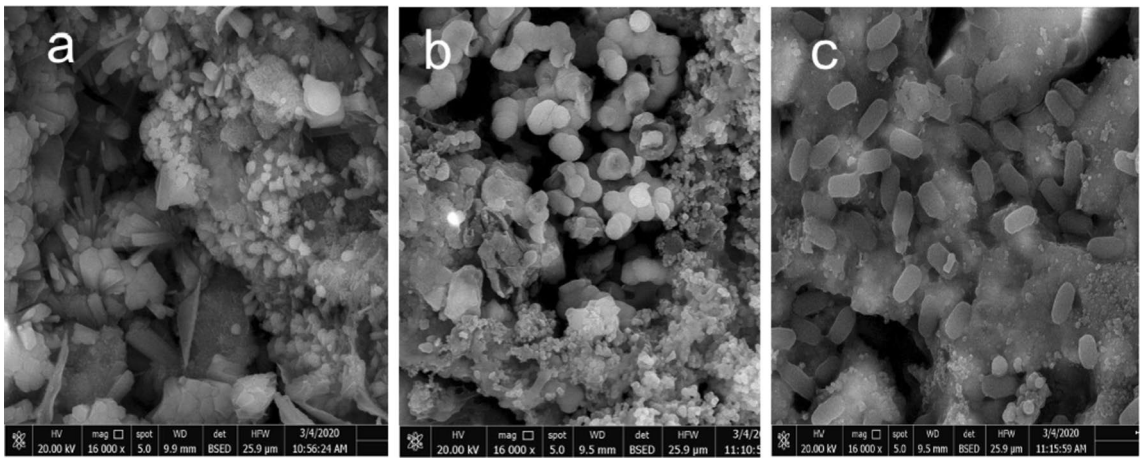

Fig. 11 SEM micrographs of 14-day sample cured in distilled water (DW plate **a**), simulated body fluid (SBF, plate **b**) and Pseudomonas aeruginosa in Mueller Hinton Broth (plate **c**)

hydrated in DW (Fig. 11, plate a) showed the highest dense and closed texture than the other hardened samples (plates b and c). The SEM micrographs shown in Fig. 11 showed these mi-crystalline fibrous of calcium silicate hydrate (CSH) gel covering the anhydrous C_3S grains and other hydrated compounds. A little amount of $Ca(OH)_2$ plates embedded in pores and between the complex hydrated phases. Investigation of the micrographs (plates a–c) shown in Fig. 11 emphasized the presence of the hexagonal crystals of the main hydration products of calcium aluminate phase (CA) that are CAH_{10} and C_2AH_8 in addition to the cubic crystals of hydrogarnet (C_3AH_6) and aluminum hydroxide (AH_3) gel formed due to the conversion process of the main hydrated phases (CAH_{10} and C_2AH_8) at 37 °C. The microstructure of sample cured in DW (Fig. 11, plate a) reveals the presence of stratlingite hydrates (C_2ASH_8) plates more than the samples cured in SBF and bacterial solutions together with a considerable amount of amorphous AH_3 gel and thin fibrous particles of C–S–H. the A mesh-like platelets of hydroxyapatite (HA) were detected in the micrograph shown in Fig. 11, plate b that are precipitated from the SBF solution on the surface of both anhydrous and hydrated grains. The micrograph of the sample cured under the microbe medium, plate c, showed a huge amounts of the Pseudomonas aeruginosa microbe embedded between the hydrated compounds and inside the microporous system. EDAX analysis of 14-day sample cured in distilled water (DW), simulated body fluid (SBF) and Pseudomonas aeruginosa in Mueller Hinton Broth, respectively, is shown in Figs. 12, 13 and 14.

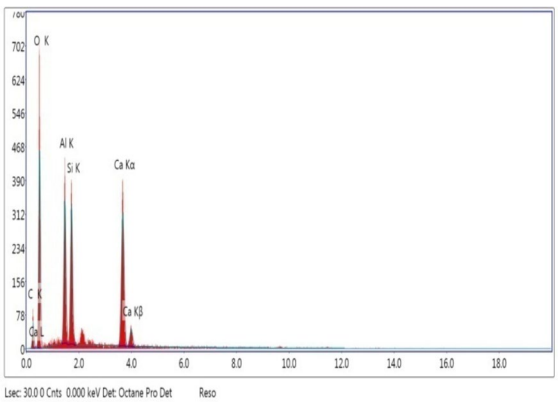

Element	Weight %	Atomic %	Net Int.	Error %
C K	13.16	19.96	14.65	14.51
O K	53.99	61.45	119.41	10.81
AlK	9.05	6.11	102.75	6.87
SiK	8.58	5.56	102.88	6.47
CaK	15.23	6.92	126.17	3.53

Fig. 12 EDAX analysis of 14-day sample cured in distilled water (DW)

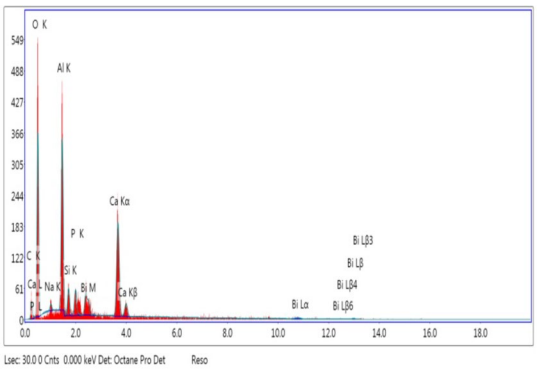

Element	Weight %	Atomic %	Net Int.	Error %
C K	8.55	13.68	6.67	18.58
O K	54.16	65.09	97.16	10.73
NaK	2.64	2.21	8.65	19.23
AlK	13.85	9.87	106.74	7.16
SiK	1.92	1.31	14.94	15.5
P K	2.07	1.29	14.92	15.11
BiM	3.89	0.36	13.61	14.32
CaK	12.92	6.2	74.52	5.02

Fig. 13 EDAX analysis of 14-day sample cured in simulated body fluid (SBF)

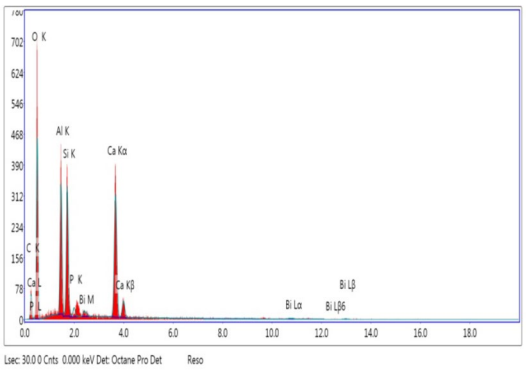

Element	Weight %	Atomic %	Net Int.	Error %
C K	12.84	19.68	14.31	14.7
O K	53.32	61.34	119.47	10.81
AlK	8.93	6.09	102.77	6.89
SiK	8.45	5.54	102.92	6.48
P K	0.59	0.35	6.06	24.16
BiM	0.77	0.07	3.96	39.15
CaK	15.09	6.93	126.19	3.6
C K	12.84	19.68	14.31	14.7

Fig. 14 EDAX analysis of 14-day sample cured in Pseudomonas aeruginosa in Mueller Hinton Broth

Cytotoxicity test

The sample was tested against the normal human epithelial cell line: -1 BJ1 (normal skin fibroblast with sample concentration range between 100 and 0.78 µg/ml) using MTT assay. The cytotoxicity data showed that the synthesized composite was highly safe to normal skin fibroblast cells with cell variability of 93.2% at 100 ppm sample concentration.

Discussion

The hydration process of the formulated bio-cement composite (1:1 C_3S and CA) proceeded immediately after mixing the dry powder with the appropriate W/S ratio (0.23) of distilled water (DW) according to the above-mentioned chemical equations (Eqs. 1, 2, 6) that is resulting in precipitation of the main hydrated compounds of CA phase (CAH_{10} and C_2AH_8) and calcium silicate hydrate (CSH) during the first few minutes of the hydration process to get the finally set samples at average setting time of 20 min that is considered acceptable for medical and dental applications. Calcium aluminate cement has an important role in improving the setting and hardening of the formulated material as it gains about 80% of its hydration reactions during the first 24 h of hydration process with DW, whereas tri-calcium silicate phase needs relatively longer setting and hardening time to get ≈80% of its hydration reactions (Bushnell-Watson and Sharp 1990; Taylor 1990). As was mentioned above in the experimental part, curing of 24 h pastes was carried out under different media in an incubator at 37 °C which will have an acceleration effect on the hydration reactions of C_3S phase resulting in more calcium silicate hydrate and calcium hydroxide [$Ca(OH)_2$] are being precipitated during the hardening process (Bushnell-Watson and Shrap 1990; Taylor 1990).

Mono-calcium aluminate phase (CA) is considered the essential aluminate phase which is responsible for the strength development. The main hydration compounds are CAH_{10} at 5–10 °C, C_2AH_8 and AH_3 at 22–35 °C and C_3AH_6 and AH_3 at a temperature over 35 °C. The conversion process of the calcium aluminate hydrate compounds is highly dependent on temperature and curing periods in which all hydration products will be converted to the cubic hydrogarnet (C_3AH_6) and gibbsite (AH_3).

The weakening of mechanical properties in hot and humid curing conditions is mainly due to the conversion of the main hydrated phases, CAH_{10} and C_2AH_8, (hexagonal crystals) to the more stable cubic hydrogarnet crystals according to Eqs. (4) and (5) (Taylor 1990; Bassyouni et al. 2014).

Tri-calcium silicate (C_3S) phase is mainly responsible for the hardening and strength development of the prepared pastes at later hydration periods through the formation of calcium silicate hydrate (CSH) according to Eq. (6). It was also found that the presence of free amorphous silica (SiO_2) in the composition of C_3S phase together with the calcium silicate hydrate due to the hydration of C_3S phase have an important role in decreasing the adverse effect of conversion process on the mechanical properties of the hardened pastes at higher curing temperature (37 °C) through forming the more stable strätlingite compound (C_2ASH_8) according to Eqs. (7)–(12) (Taylor 1990; Bassyouni et al. 2014; Matrusinovic et al. 2003):

$$2CAH_{10} \xrightarrow{(S)} C_2ASH_8 + AH_3 + 9H_2O \quad (7)$$

$$CAH_{10} + CSH \rightarrow C_2ASH_8 + 3H_2O \quad (8)$$

$$CAH_{10} \xrightarrow{(C)(S)} C_2ASH_8 + 2H_2O \quad (9)$$

$$C_2AH_8 \xrightarrow{(S)} C_2ASH_8 \quad (10)$$

$$C_2AH_8 + 2CSH + AH_3 + 3H_2O \rightarrow C_2ASH_8 \quad (11)$$

$$C_2AH_8 + AH_3 \xrightarrow{(C)(S)} C_2ASH_8 \quad (12)$$

In order to provide adequate radio opacity, bismuth oxide was added to the composition of the synthesized material as it has no adverse effect on the hydration of the two phases used in this study. Due to the fact that hydration reactions of both C_3S and CA phases are very sensitive to the ions present in the curing medium, so, in this investigation the influence of curing medium namely simulated body fluid (SBF) and Pseudomonas aeruginosa in Mueller Hinton Broth (MHB media) in comparison with distilled water (DW) on the hydration reactions and hardening process of the prepared material was studied.

The hardness Vickers values (Fig. 3) of paste samples cured under distilled water (DW) at 37 °C showed a steady increase with curing age from 1 and up to 14 days due to formation of the main hydrated products of both C_3S and CA phases according to Eqs. (1), (2) and (6) (CSH, CAH_{10} and C_2AH_8) that are responsible for the strength development (Taylor 1990). The conversion of CAH_{10} and C_2AH_8, (hexagonal crystals) to the more stable cubic hydrogarnet crystals (C_3AH_6) at 37 °C curing temperature was diminished by the reactions of free amorphous silica (SiO_2) and CSH with aluminate hydrates to give the hydraulic strätlingite compound (C_2ASH_8) of good mechanical properties according to chemical equations (Eqs. 7–12). It was found that strätlingite (C_2ASH_8) may improve the mechanical properties of CA pastes cured in hot and humid conditions as it is precipitated in the pores formed due to the conversion reactions of the metastable hexagonal crystals of CAH_{10} and C_2AH_8 that are responsible for physico-mechanical properties to the more stable C_3AH_6 (cubic crystals) and AH_3 gel that have an adverse effect on density and hardness (Scrivener and Capmas 1998; Edmonds and Majumdar 1989; Fentiman and Rashid 1990; Matrusinovic et al. 2003). The SEM micrograph of 14-day sample cured in DW represented in Fig. 10, plate a clearly showed plates of strätlingite compound (C_2ASH_8) in a highly closed and dense microstructure than the sample cured in SBF and bacterial solutions. On the other hand, the data shown in Fig. 3 illustrate that the hardness values of samples cured in SBF and bacterial media slightly decreased with the curing age, whereas sample cured in bacterial medium showed slightly higher values than those cured in SBF solution. The decrease in hardness values in case of SBF and bacterial media is mainly due to the conversion process that is very critical during later hydration ages as it adversely affect the physico-mechanical and morphological characteristics of CA phase. The conversion process results in a highly porous structure and poor mechanical properties of the hardened pastes which will be solved by tri-calcium silicate phase (C_3S) present in the synthesized material through the formation of strätlingite compound (C_2ASH_8) that is precipitated in this porous system leading to an improved hardness values for samples cured in distilled water (Fig. 3) according to chemical (Eqs. 7–12). The composition of SBF solution (Table 1) is considered a highly ionized curing medium because it composed of a number of soluble salts, namely, NaCl, $NaHCO_3$, KCl, $K_2HPO_4.3H_2O$, $MgCl_2.6H_2O$, $CaCl_2$ and Na_2SO_4 that are completely soluble in distilled water and there will be various free radicals, some of these free radical may act as an accelerator for the hydration reactions of C_3S and CA phases, while the others are considered aggressive salts for C_3S phase only because calcium aluminate phase is highly resistant to these aggressive salts (Taylor 1990). Due to the fact that hydration processes of C_3S and CA phases are very sensitive to some cations and anions (Na^+, K^+, Ca^{++}, OH^- and Cl^-), these free radicals may enhance the hydration reactions of both phases as they will act as a nucleating center for the hydrophilic

particles that pushing the hydration reactions to completion (Bushnell-Watson and Sharp 1986; Rivas Mercury et al. 2005; Shang et al. 2016). The diminished hardness values could be attributed to the acceleration effect on the hydration reactions due to the cations and anions present in SBF solution for both silicate and aluminate phases that results in an encapsulation of the huge amounts of silicate and aluminate hydrates formed on the surface of the anhydrous particles to give a more porous microstructure in addition to the conversion reactions of CA phase due to the higher curing temperature (37 °C). Mono-calcium aluminate phase possesses very good resistance to some aggressive salts like magnesium chloride and sodium sulfate (Rivas Mercury et al. 2005; Asgary and Kamrani 2008) that are present in SBF solution as given in Table 1, whereas these two aggressive salts ($MgCl_2.6H_2O$ and Na_2SO_4) are considered to have adverse effect on the hydration reactions and physico-mechanical properties of the synthesized C_3S phase because magnesium chloride and sodium sulfate salts may decompose the hydrated calcium silicates in the presence of the liberated $Ca(OH)_2$ to form $CaSO_4.2H_2O$ (gypsum) and $Mg(OH)_2$. The formed $Mg(OH)_2$ reacts with silica gel from the dissociated calcium silicate hydrates due to the sulfate attack to form magnesium silicate hydrate which possesses no binding and mechanical properties (Eq. 13) (Taylor 1990).

$$4Mg(OH)_2 + SiO_2gel \rightarrow 4MgO.SiO_2.8.5H_2O \quad (13)$$

The above-mentioned dual adverse effects on the mechanical properties of pastes cured in SBF solution may emphasize the continuous decrease in the hardness values more than those cured in bacterial solution as the Pseudomonas aeruginosa bacteria which may cause only softening of sample surface by the bacterial attack on the hydrated silicate and aluminate compounds without affecting the reaction between CSH and amorphous silica with the hydrated calcium aluminate compounds to form strätlingite compound (C_2ASH_8) which is emphasized by the presence of its plates in the micrograph of samples cured in bacterial solution (Fig. 10, plate c). The higher pH values (alkalinity) of the hydration media are mainly attributed to the liberated calcium hydroxide [$Ca(OH)_2$] from the hydration of C_3S phase (Eq. 6). The pH data illustrated in Fig. 4 indicate higher pH values for samples stored in distilled water (DW) than those cured in SBF and bacterial solutions at all curing ages that is in agreement with the hardness data in that the hydration reactions of the synthesized material were proceeded normally including the formation of strätlingite compound (Eqs. 7–12) which is responsible for the improvement in mechanical properties. The increased pH values of SBF solution than bacterial medium may be attributed to the partial dissolution of calcium aluminate compounds in the hydration medium due to the effect of cations and anions present in SBF solution (Table 1) (Taylor 1990; Bassyouni et al. 2014). Figure 5 emphasizes the highest Ca^{2+} ion values in SBF hydration medium at all curing ages due to the dissolution of both calcium silicate and calcium aluminate compounds as was discussed above, while the bacterial solution showed the lowest Ca^{2+} ion values. For the samples cured in SBF solution, there will be a great tendency for the precipitation of hydroxyapatite (HA) on the surface of the hardened pastes. The values of phosphorus ion concentration of SBF medium shown in Fig. 6 showed a decrease from 3- to 7-day samples due to the reaction of the phosphate ions present in the composition of SBF solution in the free Ca^{2+} to form hydroxyapatite (HA) on the surface of calcium aluminate hydrate and calcium silicate hydrate that emphasized the biocompatibility of the formulated material (Iftekhar et al. 2008).

The findings of XRD analysis for the 3- and 14-day samples shown in Figs. 7 and 8 are in agreement with the hardness data as the samples cured in distilled water (DW) showed the maximum decrease in the XRD peak intensities of anhydrous particles of both C_3S and CA phases that means an increasing extent of the hydration reactions more than the SBF and bacterial media. The peak intensities characteristic of the calcium aluminate and calcium silicate hydrates were higher for samples cured in DW followed by those stored in bacterial medium and the lowest intensities was recorded for the samples in SBF solution. The characteristic XRD peak of the strätlingite compound (C_2ASH_8) that is formed during the conversion reactions of CA phase according to Eqs. (7)–(12) could be found in the XRD patterns of both 3- and 7-day sample in DW more than samples stored in SBF and bacterial solutions. The XRD pattern of the samples cured in SBF solution emphasized the formation of hydroxyapatite (HA) with a slightly increased intensities for 14 days of curing age. The FTIR spectral analysis (Figs. 9, 10) are in agreement with the XRD results concerning the IR bands for the main hydrated phase of the formulated material and increased bands intensities for the 3- and 14-day samples in DW more than those stored in SBF and bacterial solutions. Also, the characteristic IR bands of anti-symmetric stretching $\acute{\upsilon}_2$ and $\acute{\upsilon}_3$ CO_3^{2-} ~850, 1400–1500 cm^{-1} were found for all samples due to the carbonation of the hydrated compounds by atmospheric CO_2. Formation of hydroxyapatite (HA) for all samples cured in SBF solution was emphasized by detection of the IR bands characteristic for symmetric stretching vibration $\acute{\upsilon}_3PO_4^{3-}$ overlapped in the region of 1050–1100 cm^{-1} and those corresponding

to the bending vibration of PO_4^{3-} at the range of 560–650 cm^{-1}. The morphology changes of the 14-day samples as influenced by the curing media are illustrated in Fig. 11. The samples cured in DW (plate a) showed the most dense and closed microstructure including the main hydrated compounds of C_3S and CA phases, namely, fibrous of CSH gel, hexagonal crystals of CAH_{10} and C_2AH_8 in addition to the cubic crystals of hydrogarnet (C_3AH_6) and aluminum hydroxide (AH_3) gel. The microstructure of samples stored in simulated body fluid solution (SBF) showed more porous structure than those cured in Pseudomonas aeruginosa microbe (MHB) medium that is in agreement with the above-mentioned findings of hardness values due to the conversion reactions in which the cubic crystals of hydrogarnet (C_3AH_6) and aluminum hydroxide (AH_3) gel that were formed at 37 °C. The stratlingite hydrate (C_2ASH_8) plates were clearly found in samples cured in DW as well as some of this plates could be also detected in pastes cured in the bacterial medium, whereas for samples stored in SBF solution it almost not found.

Conclusions

Mixing of mono-calcium aluminate phase with ultrapure tri-calcium silicate phase in ratio of 1:1 by weight improved the setting and hardening processes during the first day of hydration after mixing with distilled water. Curing of mono-calcium aluminate phase in the incubator at 37 °C results in a process called conversion in which all hydration products will be converted to the cubic hydrogarnet (C_3AH_6) and gibbsite (AH_3) in a more porous and mechanically weak structure. The results emphasized that the hydrated compounds of C_3S phase can partly solve the problem of conversion process through the formation of the more stable and highly mechanical stratlingite hydrate (C_2ASH_8) plates which was clearly detected in micrograph of samples cured in distilled water and good hardness values at all hydration ages. The morphology and mechanical properties of samples cured in simulated body fluid (SBF) have adversely affected as the cations and anions present in SBF solution result in an acceleration, aggressive and dissolution effects on the anhydrous particles and hydrated compounds of both C_3S and CA phases. The samples cured in Pseudomonas aeruginosa microbe (MHB) medium exhibited better mechanical properties and morphology features than those cured in SBF solution with a considerable amount of stratlingite hydrate (C_2ASH_8) plates embedded in the highly porous structure due to the conversion reactions of CA phases. For samples cured in SBF solution, the precipitation of hydroxyapatite (HA) on the surfaces of anhydrous and hydrated particles as well as inside the more porous system of pastes was emphasized by XRD, EDAX and SEM analyses.

Thus, it could be concluded that the prepared cements are promising for different dental application fields.

Recommendations

In vitro followed by in vivo studies for the application of these cements in different dental applications should be performed.

Abbreviations

C: CaO; A: Al_2O_3; S: SiO_2; H: H_2O; Ś: $CaSO_4{\cdot}2H_2O$; C_3A: Tri-calcium aluminate; C_3S: Tri-calcium silicate; CSH ($CaOSiO_2.4H_2O$): Calcium silicate hydrate; $Ca(OH)_2$: Calcium hydroxide; CAH_{10}: Calcium aluminate hydrate; C_2AH_8: Aluminate hydrate; AH_3: Aluminum hydroxide; C_3AH_6: Hydrogarnet; C_2ASH_8: Stratlingite hydrate; $MgO.SiO_2.8.5H_2O$: Magnesium silicate hydrate; SBF: Simulated body fluid.

Acknowledgements

Not applicable.

Author contributions

MMR performed the study design, prepared the C_3A phase, did investigations for the prepared C_3A and C_3A phases, and prepared the manuscript. SMN did hardness test. Both authors read and approved the final manuscript.

Funding

This research did not receive any specific grant from backing supports in the public, commercial, or not-for-profit sectors.

Availability of data and materials

The authors announce that the data supporting the results of this study are existing within the article.

Declarations

Ethics approval and consent to participate

Not applicable.

Consent for publication

Not applicable.

Competing interests

The authors declare that they have no competing interests.

Author details

[1]Refractories, Ceramics and Building Materials Department, National Research Centre (NRC), Dokki, Cairo 12622, Egypt. [2]Restorative and Dental Materials Department, Oral and Dental Research Institute, National Research Centre (NRC), 33 El Bohouthst. (Former El Tahrirst.), Dokki, Cairo 12622, Egypt.

Received: 18 May 2022 Accepted: 15 June 2022
Published online: 25 June 2022

References

Accorinte ML, Holland R, Reis A, Bortoluzzi MC, Murata SS, Jr Dezan E, Souza V, Alessandro LD (2008) Evaluation of mineral trioxide aggregate and calcium hydroxide cement as pulp-capping agents in human teeth. J Endod 34(1):1–6

Al-Haddad AY, Kutty MG, Abu Kasim NH, Che Ab Aziz ZA (2017) The effect of moisture conditions on the constitution of two bioceramic-based root canal sealers. J Dent Sci 12:340–346

APHA (American Public Health Association), AWWA (American Water Works Association), WEF (Water Environment Federation), Rice EW, Baird RB, Eaton AD, Clesceri LS (2017) Standards methods for the examination of water and wastewater, 23rd ed. Washington, DC
Asgary S, Kamrani FA (2008) Antibacterial effects of five different root canal sealing materials. J Oral Sci 50(4):469–474
Asgary S, Eghbal MJ, Parirokh M, Ghoddusi J, Kheirieh S, Brink F (2009) Comparison of mineral trioxide aggregate's composition with Portland cements and a new endodontic cement. J Endod 35(2):243–250
Bassyouni FA, Abu-Baker SM, Mahmoud K, Moharam M, El-Nakkady SS, Abdel-Rehim M (2014) Synthesis and biological evaluation of some new triazolo[1,5-a] quinoline derivatives as anticancer and antimicrobial agents. RSC Adv 4(46):24131–24141
Bentsen S, Seltveit A, Sanderg B (1990) Effect of microsilica on conversion of high alumina cement calcium aluminate cement. Chapman and Hall, London, p 294
Bushnell-Watson SM, Sharp JH (1986) The effect of temperature upon the setting behavior of refractory calcium aluminate cements. Cem Concr Res 16:875–884
Bushnell-Watson SM, Sharp JH (1990) On the cause of the anomalous setting behavior with respect to temperature of calcium aluminate cements. Cem Concr Res 20:677–686
Camilleri J (2007) Hydration mechanisms of mineral trioxide aggregate. Int Endod J 40(6):462–470
Camilleri J (2014) Tricalcium silicate cements with resins and alternative radiopacifiers. J Endod 40(12):2030–2035
Camilleri J, Gandolfi MG (2010) Evaluation of the radiopacity of calcium silicate cements containing different radiopacifiers. Int Endod J 43(1):21–30
Edmonds RN, Majumdar AJ (1989) The hydration of mixtures of calcium aluminate and blast furnace slag. Cem Concr Res 19:779–782
Eliopoulus GM et al (1989) Enhancement of cefotoxamine and other cephalosporins against enterococcus faecalis by blood supplemented Mueller-Hinton agar. Diagn Microbiol Infect Dis 12:149
Emara R, Elhennawy K, Schwendicke F (2018) Effects of calcium silicate cements on dental pulp cells: a systematic review. J Dent 77:18–36
Fentiman CH, Rashid S (1990) The effect of curing conditions on the hydration and strength development in fondu/slag. In: Mangabhai RJ (ed) Calcium aluminate cements. E.&F.N. Spon, London
Huang Y, Li X, Mandal P, Wu Y, Liu L, Gui H et al (2019) The in vitro antimicrobial activities of four endodontic sealers. BMC Oral Health 19(1):118
Iftekhar S, Grins J, Svensson G, Lööf J, Jarmar T, Botton GA, Andrei CM, Engqvist H (2008) Phase formation of $CaAl_2O_4$ from $CaCO_3$-Al_2O_3 powder mixtures. J Eur Ceram Soc 14:747–756
Kokubo T, Kushitani H, Sakka S, Kitsugi T, Yamamuro T (1990) Solutions able to reproduce in vivo surface-structure changes in bioactive glass-ceramic A-W. J Biomed Mater Res 24:721–734
Lee SJ, Monsef M, Torabinejad M (1993) Sealing ability of a mineral trioxide aggregate for repair of lateral root perforations. J Endod 19:541–544
Lee WE, Vieira W, Zhang S (2001) Castable refractory concretes. Int Mater Rev 46:145–167
Lenji RK, Nourbakhsh AA, Nourbakhsh N, Nourbakhsh M, Mackenzie KJ (2017) Phase formation, microstructure and setting time of MCM-48 mesoporous silica nanocomposites with hydroxyapatite for dental applications: effect of the Ca/P ratio. Ceram Int 43:12857–12862
Luz AP, Pandolfelli VC (2012) $CaCO_3$ addition effect on the hydration and mechanical strength evolution of calcium aluminate cement for endodontic applications. Ceram Int 38:1417–1425
Matrusinovic T, Sipusic J, Vrbos N (2003) Porosity- strength relation in calcium aluminate cement pastes. Cem Concr Res 33(11):1801–1806
Moreno-Vargasa YA, Luna-Ariasb JP, Flores-Floresc JO, Orozcod E, Buciod L (2017) Hydration reactions and physicochemical properties in a novel tricalcium-dicalcium silicate-based cement containing hydroxyapatite nanoparticles and calcite: a comparative study. Ceram Int 43:13290–13298
Mostafa NY, Zaki ZI, Abd Elkader OH (2012) Chemical activation of calcium aluminate cement composites cured at elevated temperature. Cem Concr Compos 34:1187–1193
Nurit J, Margerit J, Terol A, Boudeville P (1993) PH-metric study of the setting reaction of mono phosphate monohydrate/calcium oxide-based cements. J Mater Sci Mater Med 13:1007–1014
Parreira RM, Andrade TL, Luz AP, Pandolfelli VC, Oliveira IR (2016) Calcium aluminate cement-based compositions for biomaterial applications. Ceram Int 42(10):11732–11738
Primus C, Gutmann JL, Tay FR, Fuks AB (2022) Calcium silicate and calcium aluminate cements for dentistry reviewed. J Am Ceram Soc 105:1841–1863
Rivas Mercury JM, De Aza AH, Pena P (2005) Synthesis of CaAl2O4 from powders: particle size effect. J Eur Ceram Soc 25(14):3269–3279
Sarkar NK, Caicedo R, Ritwik P, Moiseyeva R, Kawashima I (2005) Physicochemical basis of the biologic properties of mineral trioxide aggregate. J Endod 31(2):97–100
Scrivener KL, Capmas A (1998) Calciumaluminate cements. In: Hewlett PC (ed) Lea's chemistry of cement and concrete. Arnold, Paris, pp 1–12
Shang X, Ye G, Zhang Y, Li H, Hou D (2016) Effect of micro-sized alumina powder on the hydration products of calcium aluminate cement at 40°C. Ceram Int 42:14391–14394
Taylor HFW (1990) Cement chemistry. Academic Press, London
Ukrainczyk N, Matusinovic T, Kurajica S, Zimmermann B, Sipusic J (2007) Dehydration of a layered double hydroxide-C_2AH_8. Thermochim Act 464:7–15
Wang X, Sun H, Chang J (2008) Characterization of Ca_3SiO_5/$CaCl_2$ composite cement for dental application. Dent Mater 24(7):4–82

Publisher's Note